Mathematical Biosciences 282 (2016) 82–90

Contents lists available at ScienceDirect

Mathematical Biosciences

journal homepage: www.elsevier.com/locate/mbs

Kinetics of the formation of a protein corona around nanoparticles

Vladimir P. Zhdanov[a,b,*], Nam-Joon Cho[a]

[a] School of Materials Science and Engineering, Nanyang Technological University, Singapore 639798, Singapore
[b] Boreskov Institute of Catalysis, Russian Academy of Sciences, Novosibirsk 630090, Russia

ARTICLE INFO

Article history:
Received 30 June 2016
Revised 26 September 2016
Accepted 28 September 2016
Available online 6 October 2016

Keywords:
Nanoparticles
Proteins
Adsorption kinetics
Diffusion limitations
Vroman effect
Denaturation

ABSTRACT

Interaction of metal or oxide nanoparticles (NPs) with biological soft matter is one of the central phenomena in basic and applied biology-oriented nanoscience. Often, this interaction includes adsorption of suspended proteins on the NP surface, resulting in the formation of the protein corona around NPs. Structurally, the corona contains a "hard" monolayer shell directly contacting a NP and a more distant weakly associated "soft" shell. Chemically, the corona is typically composed of a mixture of distinct proteins. The corresponding experimental and theoretical studies have already clarified many aspects of the corona formation. The process is, however, complex, and its understanding is still incomplete. Herein, we present a kinetic mean-field model of the formation of the "hard" corona with emphasis on the role of (i) protein-diffusion limitations and (ii) interplay between competitive adsorption of distinct proteins and irreversible reconfiguration of their native structure. The former factor is demonstrated to be significant only in the very beginning of the corona formation. The latter factor is predicted to be more important. It may determine the composition of the corona on the time scales comparable or longer than a few hours.

© 2016 Elsevier Inc. All rights reserved.

1. Introduction

Adsorption of proteins on solid surfaces is studied already several decades (reviewed in [1–8]). The general concepts used to interpret the corresponding kinetics are considered to be well established and can be summarized as follows:

(i) The size of proteins is relatively large (a few nm) and the coefficients of protein diffusion, determined in solution by hydrodynamics, are low, while the adsorption process itself is often rapid, because the corresponding activation energy is usually small; and accordingly the whole adsorption process and especially its onset is often globally controlled by protein diffusion [8].

(ii) Adsorption of proteins is accompanied by the reconfiguration of their native structure. This process may be reversible (for the corresponding models, see e.g. Ref. [9] or Section 5.2 in review [4]). Often, it occurs rapidly during adsorption and/or just after adsorption, the corresponding changes of the protein structure may me modest, and mechanistically it can be included into the adsorption step. Alternatively, the reconfiguration may me appreciable (up to full denaturation) and take place on the time scale much longer than that characterizing the onset of adsorption. Under such circumstances, it should mechanistically be described as a distinct step characterized by its own rate constant (as it was first done by Lundström [10]).

(iii) On the time scale of conventional experiments, diffusion of adsorbed proteins is usually relatively rapid (the diffusion length is larger than the protein size) [11]. Mechanistically, this process is expected to include local temporal rearrangements of the protein structure.

(iv) One of the consequences of reconfiguration and surface diffusion of adsorbed proteins is that with increasing coverage the already adsorbed proteins may adjust their location and structure for additional adsorption of newly arriving proteins. This costs energy and collectively can be described in terms of lateral protein–protein interactions (i.e., the interactions along the surface), which influence the protein binding energy as well as the activation energy for adsorption. Direct electrostatic interaction between charged parts of adsorbed proteins can also contribute to their lateral interaction.

(v) Adsorption of proteins is reversible and eventually accompanied by their desorption. The latter process may, however, be slow (especially if the denaturation is appreciable), and on the time scale of a given experiment the adsorption may be apparently irreversible.

(vi) In the case of coadsorption of proteins, the whole process starts by adsorption of the proteins with the highest adsorption rate. Such proteins are usually relatively small and

* Corresponding author at: Boreskov Institute of Catalysis, Russian Academy of Sciences, Novosibirsk 630090, Russia.
E-mail address: zhdanov@catalysis.ru (V.P. Zhdanov).

http://dx.doi.org/10.1016/j.mbs.2016.09.018
0025-5564/© 2016 Elsevier Inc. All rights reserved.

their binding energy is relatively low. The binding energy of proteins with larger size and smaller adsorption rate is often higher. Thermodynamically, the adsorption of the latter proteins is more favorable. For this reason, the initial high uptake of the proteins with low binding energy eventually starts to decrease due to the loss of competition for the binding site, and their final uptake may be appreciably smaller than the maximum one. This feature of protein coadsorption kinetics is referred to as the Vroman effect [12,13].

With the rapid development of nanoscience during the past decade, the interaction of proteins with metal (e.g., gold), oxide (e.g., silica and titana) and chemically fabricated (e.g., polystyrene) NPs has attracted appreciable attention due to interesting basic features, various potential applications of NPs, including e.g., targeted drug delivery, hyperthermia therapy, contrast imaging, fabrication of virus-like particles, and resolution of the potential threat of nanotechnological devices to organisms and the environment (reviewed in [14–21]; see also a recent article by Chen et al. [22]). In biological fluids, adsorption of selected proteins on such NPs results in the formation of the so-called protein corona that dramatically influences the function of NPs in biological systems. The onset of this process is usually very fast, but the whole process may take many hours or days due to slow reconfiguration and exchange of proteins at high coverage. Many related experiments were focused on the structure and composition of the corona formed after a certain interval of time (typically from about one hour to a few days). Structurally, the corona was found to contain a "hard" part, consisting of a near-monolayer of strongly bound proteins, and a "soft" part located on top and consisting of a weakly associated and rapidly exchanging layer of proteins. In practically important situations (e.g., in human blood plasma [23]), the number of distinct proteins is large but, due to the competition for the binding sites, the corona typically contains only some of them. In the case of silica NPs in blood plasma, for example, the corona consists primarily of 20 proteins (see Table 1 in [15]).

Detailed experimental studies of the kinetics of the corona formation are still not numerous (see, e.g., Refs. [24–28]). The focus is typically on the dependence of the integral protein uptake on time, because the tools to track the composition of the corona as a function of time are still limited. The experiments resolving the temporal populations of individual proteins are just beginning [27]. The available models of the kinetics of the corona formation (reviewed in [29,30]) are of two complementary categories including, respectively, coarse-grained atomistic simulations with emphasis on the dynamical aspects [31–34] and conventional mean-field (MF) kinetic models focused on the "hard" part of the corona with emphasis on competitive adsorption [35,36] or on the "soft" part [37].

In general, the kinetics of the formation of a protein corona around NPs depend or may depend on numerous factors. Herein, we present a general MF kinetic model of the formation of the "hard" part of the protein corona (Section 2). Compared to the already available models, it scrutinizes in more detail the onset of the kinetics or, more specifically, the role of diffusion limitations (Section 2) and the final stage of the kinetics with the interplay between competitive adsorption, desorption and irreversible reconfiguration of different proteins (Section 3). From various points of view (e.g., in applications), the final stage of the kinetics is more important than the onset. The reconfiguration of some of the proteins during the final stage of the kinetics is expected to take place if the protein binding energy is significant. This is often the case for metal and oxide NPs. For this reason, our model is oriented to metal and oxide NPs. The model itself is relatively simple and makes it possible to understand likely general trends in the kinetics under consideration. The cumbersome details related to diffusion limitations are given in Appendix A and may be omitted if one is not interested in math. The expected scale of deviations from the MF approximation at high coverage is illustrated in Appendix B by using Monte Carlo (MC) simulations (this Appendix may be omitted as well if one is not interested in math). Focusing on the general interplay of the kinetic steps, we do not take into account many specific factors which may be important for specific nanoparticles and/or proteins. Some of such factors are briefly discussed in Section 4. Finally, we summarize our key findings in Section 5.

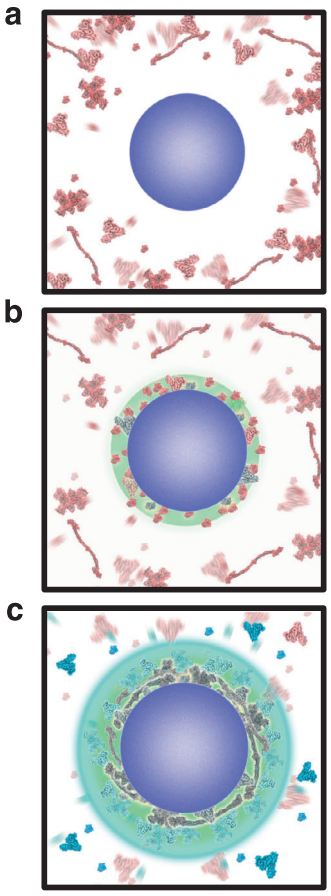

Fig. 1. Schematic view of the formation of the hard protein corona around a nanoparticle in blood plasma. The panels show the cross section of a nanoparticle surrounded by adsorbed proteins. For the sake of simplicity, the proteins exhibited include only Fibrinogen (large sized protein), Vitronectin and Human Serum Albumin (intermediate sized), and Cytochrome C (small sized proteins). The whole process is divided into three stages: (a) a nanoparticle is introduced into plasma, (b) smaller proteins (HSA and Cyt C) adsorb first and some are denatured, and (c) eventually, larger proteins replace the smaller ones (Vroman effect) and then undergo denaturation to achieve irreversible adsorption. Native plasma proteins are represented in red (online). Denatured adsorbed proteins are shown in gray. Desorbed proteins are represented in blue. The hard corona is emphasized with a green halo. The soft corona is differentiated by a cyan colored halo (with associated proteins in the same color). (For interpretation of the references to color in this figure legend, the reader is referred to the web version of this article.)

2. General equations

In our model, a NP is considered to be spherical (Fig. 1). The adsorption of each protein is described in the two-state approximation (as originally proposed by Lundström [10] and reviewed in Ref. [8]), i.e., a protein is considered to be adsorbed either in the native or in the altered (denatured) state. The transition kinetics from the former to the latter state is assumed to be irreversible and to obey the first-order law with a correction taking saturation of the adsorbed overlayer into account. Reconfiguration of

the protein native structure occurring during adsorption and/or rapidly and reversibly just after adsorption is included into the adsorption step. To describe the adsorption kinetics, we operate with the populations of adsorbed proteins in these states, n_i and n_i^*, where the subscript i characterizes distinct proteins (in principle, one could operate with surface concentrations; on NPs, the protein populations are, however, relatively small, and accordingly these variables are physically preferable). At saturation, the corresponding surface areas per protein are defined to be s_i and s_i^*, respectively. At arbitrary populations of adsorbed proteins, the total surface coverage of a NP is defined as

$$\Theta = \left(\sum_i s_i n_i + \sum_i s_i^* n_i^*\right)/4\pi R^2, \tag{1}$$

where $R = \rho + \langle a\rangle$ is the radius of the sphere corresponding on average to the location of the centers of the protein masses, $4\pi R^2$ is the area of this sphere, ρ is the NP radius, and $\langle a\rangle$ is one half of the average effective protein thickness in the direction perpendicular the nanoparticle surface (for spherically shaped proteins, $\langle a\rangle$ can be identified with the average effective protein radius; in reality, one often has $\rho \gg \langle a\rangle$ and accordingly $R \simeq \rho$). Due to steric constrains, the adsorption and denaturation rate are assumed to be proportional to the fraction of the uncovered surface, i.e., to $1-\Theta$.

With the specification above, the MF kinetic equations for the populations are as follows

$$dn_i/dt = 4\pi R^2 k_i(1-\Theta)c_i(R+\langle a\rangle) - \kappa_i n_i - r_i(1-\Theta)n_i, \tag{2}$$

$$dn_i^*/dt = r_i(1-\Theta)n_i, \tag{3}$$

where k_i are the adsorption rate constants (these constants are considered to correspond to the adsorption rate per unit area, and accordingly the total adsorption rate of each protein is proportional $4\pi R^2$), κ_i and r_i are the desorption and denaturation rate constants, $1-\Theta$ is the above-introduced fraction of the uncovered surface, and $c_i(R+\langle a\rangle)$ are the protein concentrations (per unit volume) at the distance $R+\langle a\rangle$ from the NP center.

The use of the MF approximation [Eqs. (1)–(3)] implies that the correlations in the arrangement of adsorbed proteins are not crucial for the understanding the adsorption kinetics. One of the factors justifying this assumption is diffusion of adsorbed proteins. The so-called random sequential adsorption models, implying immobile adsorbates, represent an alternative approximation (reviewed in detail in [38]; for the corresponding models focused on co-adsorption, see Refs. [39–41]). In reality, as already noticed in the Introduction, diffusion of proteins adsorbed on different substrates is often rather rapid especially on the nano-scale length [11], and accordingly the MF approximation is a more reasonable basis for the analysis.

One of the shortcomings of the MF approximation is that the effect of saturation on adsorption and denaturation is described by using the simplest prescription that the corresponding rates are proportional to $1-\Theta$. Strictly speaking, this prescription should be corrected at high coverage even in the case of adsorption not complicated by lateral interactions between adsorbed proteins (see Appendix B). The corresponding corrections are, however, not expected to change our main qualitative conclusions. Concerning lateral interactions, we note that our generic analysis is aimed at the biologically relevant conditions when the charges of proteins (both in solution and adsorbed state) are small and accordingly the lateral interactions are typically modest (see Section 4). To fit experimental data, one can use this or more complex approximations taking, e.g., lateral protein–protein interactions into account.

Employing Eq. (2) on the length scale comparable to that of a NP implies that the concentration $c_i(R+a)$ is calculated as the average for the ensemble of NPs, i.e., this is ensemble-averaged concentration. According to (2), the net rate of adsorption of protein i to the NP surface is given by

$$J_i = 4\pi R^2 k_i(1-\Theta)c_i(R+\langle a\rangle) - \kappa_i n_i. \tag{4}$$

On the other hand, this rate should be equal to the protein diffusion flux at $r = R+\langle a\rangle$, where r is the radial coordinate. The latter flux is given by the solution of the corresponding diffusion equation and can be represented as [see Eq. (30) in Appendix A and take into account that a and $\rho+2a$ can there be replaced by $\langle a\rangle$ and $\rho+2\langle a\rangle \equiv R+\langle a\rangle$, because here we are interested in the average values]

$$J_i = 4\pi R D_i[c_i^\circ - c_i(R+\langle a\rangle)], \tag{5}$$

where c_i° is the concentration in solution far from a NP. Using (4) and (5), we have

$$4\pi R^2 k_i(1-\Theta)c_i(R+\langle a\rangle) - \kappa_i n_i = 4\pi R D_i[c_i^\circ - c_i(R+\langle a\rangle)]. \tag{6}$$

This equation yields

$$c_i(R+\langle a\rangle) = \frac{4\pi R D_i c_i^\circ + \kappa_i n_i}{4\pi R D_i + 4\pi R^2 k_i(1-\Theta)}. \tag{7}$$

Substituting this expression into Eq. (2) results in

$$dn_i/dt = A_i c_i^\circ - B_i n_i - r_i(1-\Theta)n_i, \tag{8}$$

where

$$A_i \equiv \frac{4\pi R D_i k_i(1-\Theta)}{D_i/R + k_i(1-\Theta)} \quad \text{and} \quad B_i \equiv \frac{\kappa_i D_i/R}{D_i/R + k_i(1-\Theta)} \tag{9}$$

are the effective adsorption and desorption rate constants taking the diffusion limitations into account. At the onset of adsorption, Θ is low. If in addition k_i is sufficiently large, one may have $k_i(1-\Theta) \gg D_i/R$. In this case, the adsorption and desorption of protein i are limited by diffusion in solution, and the corresponding rate constants (9) can be represented as

$$A_i \simeq 4\pi R D_i \quad \text{and} \quad B_i \simeq \kappa_i D_i/[R_i k_i(1-\Theta)]. \tag{10}$$

If $k_i(1-\Theta) \ll D_i/R$ (this is the case at the late stage of the corona formation), both processes are kinetically limited, and one has

$$A_i \simeq 4\pi R^2 k_i(1-\Theta) \quad \text{and} \quad B_i \simeq \kappa_i. \tag{11}$$

To present the results of numerical calculations, it is convenient to introduce the partial protein coverages defined as

$$\theta_i = s_i n_i/4\pi R^2 \quad \text{and} \quad \theta_i^* = s_i^* n_i^*/4\pi R^2. \tag{12}$$

The kinetic equations for these coverages can be obtained by multiplying Eqs. (3) and (8) by $s_i^*/4\pi R^2$ and $s_i/4\pi R^2$, respectively, i.e.,

$$d\theta_i/dt = \mathcal{A}_i s_i c_i^\circ - B_i\theta_i - r_i(1-\Theta)\theta_i, \tag{13}$$

$$d\theta_i^*/dt = (s_i^*/s_i)r_i(1-\Theta)\theta_i, \tag{14}$$

where

$$\mathcal{A}_i \equiv \frac{A_i}{4\pi R^2} \equiv \frac{(D_i/R)k_i(1-\Theta)}{D_i/R + k_i(1-\Theta)}. \tag{15}$$

Using Eqs. (13) and (14), we illustrate below the specifics of the kinetics under consideration.

3. Results of calculations

In vivo or related experiments, the solution typically contains various proteins, and in general the number of the corresponding kinetic equations and rate constants may be enormous. To reduce the number of model parameters, we will operate on the coarse-grained level. In particular, we divide the whole protein population into three subpopulations, which are different with respect to size,

binding energies and denaturation. The proteins belonging to the first subpopulation (e.g., Lysozyme, β-Lactoglobulin, or α-Chymotrypsin [4]) are considered to be relatively small and rigid compared to those of the second and third subpopulations. Their binding energy is considered to be relatively small as well, and during adsorption they are assumed to be intact. The proteins belonging to the second and third subpopulation (e.g., Albumin, Transferrin, and Immunoglobulins [4]) are considered to be larger and their binding energies are larger as well. Some of these proteins remain intact after adsorption. Such proteins form the second subpopulation. Denaturation is admitted only for the proteins of the third subpopulation.

With the specification above, Eqs. (13) and (14) are reduced to

$$d\theta_1/dt = \mathcal{A}_1 s_1 c_1^\circ - B_1\theta_1, \tag{16}$$

$$d\theta_2/dt = \mathcal{A}_2 s_2 c_2^\circ - B_2\theta_2, \tag{17}$$

$$d\theta_3/dt = \mathcal{A}_3 s_i c_3^\circ - B_3\theta_i - r_3(1-\Theta)\theta_3, \tag{18}$$

$$d\theta_3^*/dt = (s_3^*/s_3) r_3(1-\Theta)\theta_3. \tag{19}$$

These equations were numerically integrated assuming that at $t = 0$ the NP is free of proteins, i.e., $\theta_1(0) = \theta_2(0) = \theta_3(0) = \theta_1^*(0) = 0$.

To use the dimensionless rate constants, we normalize them to the desorption rate constant of the proteins belonging to the first population, i.e., to κ_1. In particular, the parameters characterizing adsorption are set as $s_1 k_1 c_1^\circ/\kappa_1 = 5$, $s_2 k_2 c_2^\circ/\kappa_1 = 1$, and $s_3 k_3 c_3^\circ/\kappa_1 = 1$. Using these parameters, we imply that the concentrations of proteins of different populations are comparable, while in analogy with the activation energies for desorption the activation energy of adsorption of proteins belonging to the first subpopulation is somewhat smaller compared to those of the proteins of the second and third subpopulations, and accordingly k_1 is larger than k_2 and k_3 (as it is considered in the explanation of the Vroman effect). The difference in the values of diffusion coefficients of proteins is neglected, and the ratios of the rate constants characterizing diffusion and adsorption are fixed as $D_1/(Rk_1) = 1$, $D_2/(Rk_2) = 5$, and $D_3/(Rk_3) = 5$. The ratio s_3^*/s_3 is considered to be equal to 2. The governing parameters are chosen to be κ_2/κ_1, κ_3/κ_1, and r_3/κ_1. These parameters characterize slow steps of desorption and denaturation.

With the parameters chosen, the NP is always first rapidly covered primarily by proteins forming the first subpopulation and partly by proteins forming the second and third subpopulations. Then, the coverage of proteins forming the first subpopulation starts to decrease while the coverages of proteins forming the second and third subpopulations increase. The denaturation is negligible during this stage. As a whole, these features illustrate the Vroman effect. The corresponding details depend on the ratios of the governing parameters. The subsequent long phase includes protein denaturation.

From the tutorial point of view, it is instructive first to show (Fig. 2) what may happen if the rate constants of slow steps of desorption and denaturation are equal, $\kappa_2/\kappa_1 = \kappa_3/\kappa_1 = r_3/\kappa_1 = 0.1$. In this case, after rapid initial adsorption, one can observe a relatively short Vroman phase with simultaneous increase of the coverage of proteins forming the second and third subpopulation. Then, the coverage of the surface by the denaturated protein, θ_3^*, slowly increases, while the coverages θ_1, θ_2, and θ_3 decrease in parallel.

As a second example, we show (Fig. 3) the kinetics calculated for the case when the rate constant of desorption of proteins forming the second subpopulation is chosen to be low compared to the other rate constants, $\kappa_2/\kappa_1 = 0.02$, $\kappa_3/\kappa_1 = 0.1$, and

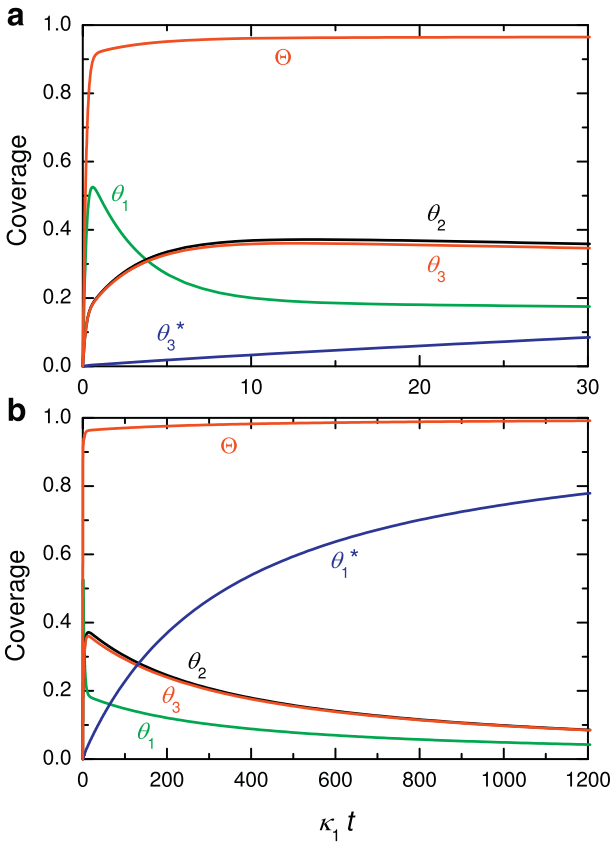

Fig. 2. Kinetics of the formation of the "hard" protein corona around a nanoparticle: protein coverages as a function of time for $\kappa_2/\kappa_1 = \kappa_3/\kappa_1 = r_3/\kappa_1 = 0.1$. Panel (a) shows the initial and Vroman phases. Panel (b) exhibits the whole kinetics.

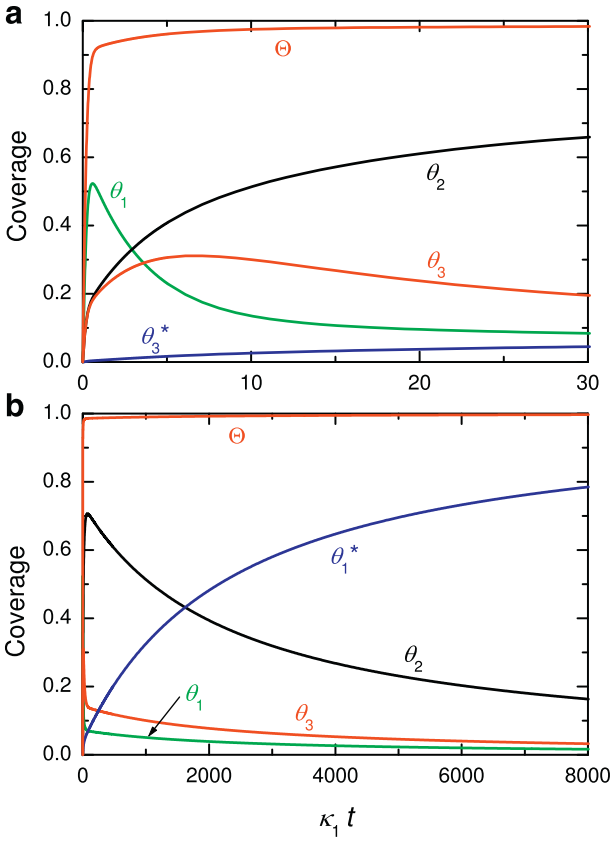

Fig. 3. As Fig. 2 for $\kappa_2/\kappa_1 = 0.02$, $\kappa_3/\kappa_1 = 0.1$, and $r_3/\kappa_1 = 0.1$.

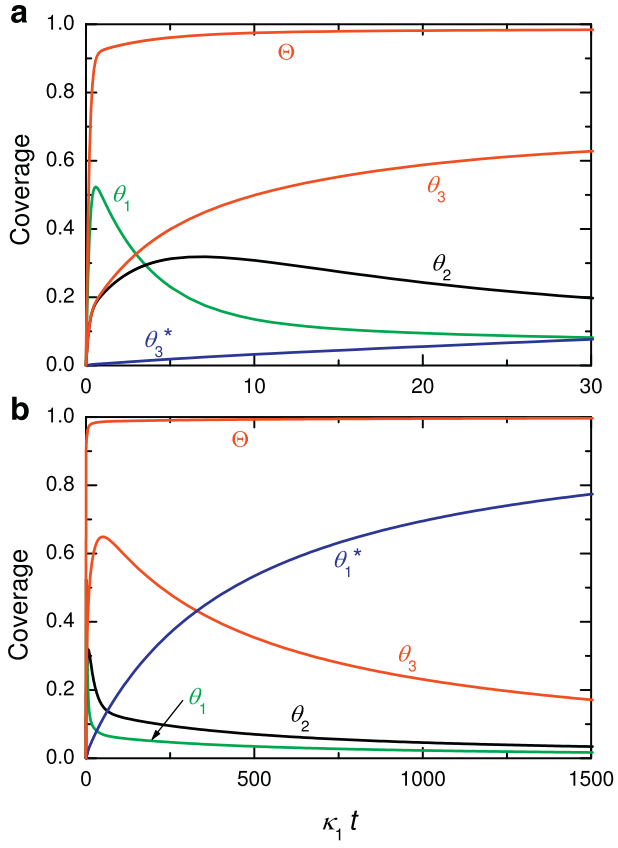

Fig. 4. As Fig. 2 for $\kappa_2/\kappa_1 = 0.1$, $\kappa_3/\kappa_1 = 0.02$, and $r_3/\kappa_1 = 0.1$.

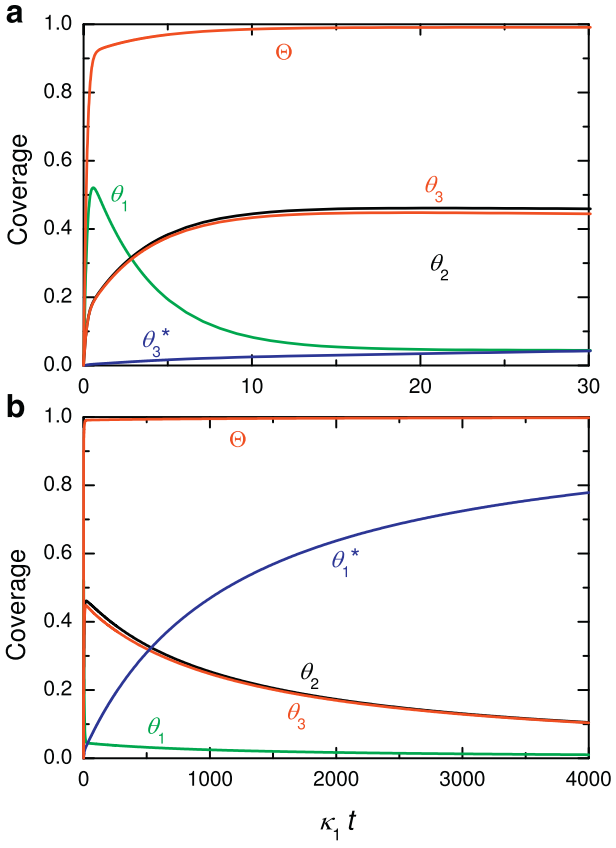

Fig. 5. As Fig. 2 for $\kappa_2/\kappa_1 = 0.02$, $\kappa_3/\kappa_1 = 0.02$, and $r_3/\kappa_1 = 0.1$.

$r_3/\kappa_1 = 0.1$. In this case, the Vroman phase shows a decrease of θ_1 accompanied by an increase of θ_2 and θ_3 and then a decrease of θ_1 and θ_3 accompanied by an increase of θ_2. Then, θ_3^* slowly increases, while θ_1, θ_2, and θ_3 decrease in parallel.

In the third example (Fig. 4), the rate constant of desorption of proteins forming the third subpopulation is low compared to the other rate constants, $\kappa_2/\kappa_1 = 0.1$, $\kappa_3/\kappa_1 = 0.02$, and $r_3/\kappa_1 = 0.1$. With these parameters, the Vroman phase exhibits a decrease of θ_1 accompanied by an increase of θ_2 and θ_3 and then a decrease of θ_1 and θ_2 accompanied by an increase of θ_3. Then, θ_3^* slowly increases.

As a final example, we show (Fig. 5) the kinetics calculated for the case when the rate constants of desorption of proteins forming the second and third subpopulation are low compared to the denaturation rate constant, $\kappa_2/\kappa_1 = 0.02$, $\kappa_3/\kappa_1 = 0.02$, and $r_3/\kappa_1 = 0.1$. In this situation, the kinetics are qualitatively similar to those presented in Fig. 2. The duration of the final phase is, however, much longer, because the total protein coverage during this phase is high, and the denaturation is very slow.

4. Additional factors

Our presentation above has been focused on protein-diffusion limitations and the interplay between protein adsorption, desorption and irreversible reconfiguration. The model employed has allowed us to scrutinize the role of these factors. Here, we briefly discuss a few specific factors which have not been taken into account.

One factor is a protein charge composed of charges of some amino-acid residues. It depends on pH and ionic strength of the solution and may (i) influence the protein binding energy, (ii) contribute to lateral interaction between adsorbed proteins, and (iii) influence the adsorption kinetics both in the kinetically and diffusion-limited regimes. In general, this factor may or may not be important and the corresponding models should be focused on specific proteins (see e.g. the treatments focused on conventional protein adsorption [42–45]). With this reservation, we note that the protein binding energy determines the value of the detachment rate constant and accordingly is taken into account already at the MF level. The repulsive or attractive lateral interaction may result in correlation in arrangement of proteins, e.g., in aggregation. In principle, most proteins are able to aggregate, although this is not required for their natural function, as evidenced by the small number of proteins that aggregate at biologically relevant conditions [46,47]. In other words, this means that under such conditions the lateral interactions are typically relatively weak and can be taken into account at the MF level by introducing the dependence of the activation energies of adsorption, desorption and denaturation on the populations of adsorbed proteins (by analogy with conventional models of adsorption of biomolecules [48]). The corresponding modification of the model proposed is not expected to change our qualitative conclusions. The length scale of the charge-related protein–protein interactions is smaller or comparable to the protein size. The diffusion limitations discussed in our study takes place at larger length scale. Thus, from the latter perspective, the role of the protein charge is not expected to be significant either.

To describe steric constraints, we have used the simplest approximation based on the introduction of the areas, s_i and s_i^*, which are locked by proteins [see the factor Θ defined by Eq. (1) or the factor $(1-\Theta)$ in Eqs. (2) and (3)]. These factors are assumed to be independent of the arrangement of proteins. As already noticed, the shortcomings of this approximation at high coverage are illustrated in Appendix B. Here, we add that in reality the smaller proteins can be located partly underneath

the larger ones so that their projections on the NP surface are slightly overlapping. In principle, this effect can be introduced into a model by representing proteins e.g. by truncated spheres. Its role is, however, not expected to be dramatic.

In our analysis, the NP surface was assumed to be uniform. This approximation may or may not be applicable. The shape of metal NPs, for example, is determined by the Wulff rule. In particular, such NPs contain the (111) and (100) facets separated be edges. The integral area of the (100) facets is, however, relatively small, and, if the cooperative effects in the protein adsorption are not appreciable, the role of these facets and edges is expected to be not appreciable either. If on the other hand the adsorption occurs via aggregate nucleation and growth, and the nucleation takes place primarily on the (100) facets, these facets may play an important role.

5. Conclusion

We have presented a kinetic MF model of the formation of the "hard" protein corona around NPs with emphasis on the role of (i) protein-diffusion limitations and (ii) interplay between competitive adsorption of distinct proteins and the reconfiguration of their native structure. Our key novel findings are as follows.

First, our analysis of protein diffusion indicates that the role of the slowdown of this process near the interface is minor. In fact, one can use the conventional diffusion equation in order to describe the process. In our treatments, we have derived general expressions for effective adsorption and desorption rate constant taking diffusion limitations into account. The expressions are applicable at arbitrary rate of diffusion, i.e., can be used when the diffusion controls adsorption or desorption as well as when the diffusion limitations are negligible. Practically, these limitations may be appreciable only in the very beginning of adsorption.

Second, our calculations show that during the Vroman phase the protein denaturation may be nearly negligible. In contrast, the final third long period of adsorption may be determined by denaturation, and if this is the case the coverages of proteins in the native states slowly decrease in parallel with increase of the coverage of the protein in the denatured state. In the current literature (reviewed in [14]), the role of the Vroman effect in the corona formation is well appreciated. The role of denaturation or, in other words, conformational changes is mentioned (reviewed in [14]) but was not theoretically illustrated in detail at it has been done here.

In addition, using Monte Carlo (MC) simulations, we have briefly illustrated the expected scale of deviations from the MF approximation at high coverage (Appendix B).

Taken together, our results clarify the mechanistic aspects of the protein-corona formation, and potentially the equations derived can be used to fit experimental data.

Acknowledgments

The authors wish to acknowledge support from the National Research Foundation of Singapore. V.P.Zh. is a recipient of the Tan Chin Tuan Exchange Fellowship at Nanyang Technological University.

Appendix A. Diffusion limitations

As a complementary part of the analysis presented in Section 2, we describe here protein diffusion towards a NP. Formally, this is one of the aspects of the theory of diffusion-limited rate processes, and the corresponding treatments has a long history since the seminal article by Smoluchowski [49] (see other seminal articles [50,51], recent treatments focused on the role of stochasticity [52] and crowding [53], and references therein). Customarily, the analysis of such processes is based on the use of the conventional diffusion equation with the constant diffusion coefficient, given by hydrodynamics for the bulk,

$$D_\circ = k_B T/6\pi\eta a, \tag{20}$$

where k_B is the Boltzmann constant, T the temperature, a the reactant radius (in our context, this is a protein radius), and η the viscosity coefficient. According to hydrodynamics, the coefficient of diffusion near the solution-solid interface is, however, smaller. For a flat interface, it can be represented as [54,55]

$$D(h) = \frac{6h^2 + 2ha}{6h^2 + 9ha + 2a^2} D_\circ, \tag{21}$$

where $h \equiv z - a$ is the minimal distance between the reactant surface and the solid surface (z is the coordinate of the reactant center with respect to the interface). In fact, D vanishes at $h \to 0$. This effect can appreciably influence the rate of diffusion-limited rate processes [56]. Here, we are interested in the expression of the protein diffusion flux at $r = R + \langle a\rangle \equiv \rho + 2\langle a\rangle$ (r is the radial coordinate with respect to the center of a NP) via the protein concentrations far and near the NP surface in order to balance the flux given by Eq. (4). In this context, we scrutinize whether the slowdown of diffusion near the NP surface significantly modify the diffusion flux.

In our analysis, we take into account that usually the NP radius, ρ, is appreciably larger than the protein radius, a (to simplify the designations, we omit here the subscript i characterizing the protein type and use a and $\langle a\rangle$ interchangeably) and, accepting expression (21), fit it as [56] (Fig. 6)

$$D(r) = \begin{cases} (r - \rho - a)\lambda^{-1} D_\circ & \text{at } \rho + a \le r \le \rho + a + \lambda, \\ D_\circ & \text{at } r \ge \rho + a + \lambda, \end{cases} \tag{22}$$

where $r - \rho - a \equiv h$ is the minimal distance between the protein surface and the NP surface, and $\lambda = 4a$ is the fitting parameter. In analogy with Eq. (21), Eq. (22) predicts $D \propto r - \rho - a$ at $r \simeq \rho + a$ and $D = D_\circ$ at $r \gg \rho + a$.

To describe protein diffusion, we consider that the protein distribution around a NP is spherically symmetric on average and employ the steady-state approximation. The latter approximation used widely since Smoluchowski's study [49] is reasonable, because the time scale of the transition to the steady-state regime is short, and the protein uptake during this transition is negligible. In combination with (22), this approximation yields at $r \ge \rho + a + \lambda$ the conventional expressions for the protein diffusion flux (per a NP) and concentration

$$J = 4\pi r^2 D_\circ \frac{dc}{dr}, \tag{23}$$

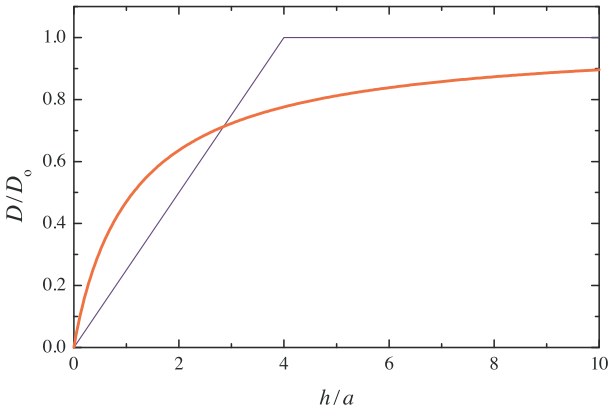

Fig. 6. Diffusion coefficient as a function of the distance, h ($h \equiv r - \rho - a$), between a protein and a nanoparticle. The thick and thin lines correspond to expressions (21) and (22), respectively.

$$c(r) = c_\circ - \frac{J}{4\pi D_\circ r}, \tag{24}$$

where $c_\circ$ is the protein concentration at $r \gg \rho + a$ (this concentration can be identified with the average concentration). At $r \leq \rho + a + \lambda$, the diffusion flux is given by

$$J = 4\pi r^2 (r - \rho - a)\lambda^{-1} D_\circ \frac{dc}{dr}. \tag{25}$$

In this expression, r^2 can be replaced by $(\rho + a)^2$, because r is close to $\rho + a$, i.e.,

$$J = 4\pi (\rho + a)^2 (r - \rho - a)\lambda^{-1} D_\circ \frac{dc}{dr}, \tag{26}$$

and then the integration yields

$$c(r) = c(\rho + 2a) + \frac{\lambda J}{4\pi (\rho + a)^2 D_\circ} \ln\left(\frac{r - \rho - a}{a}\right). \tag{27}$$

At $r = \rho + a + \lambda$, concentrations (24) and (27) should coincide, i.e.,

$$c_\circ - \frac{J}{4\pi D_\circ (\rho + a + \lambda)} = c(\rho + 2a) + \frac{\lambda J}{4\pi (\rho + a)^2 D_\circ} \ln(\lambda / a). \tag{28}$$

On the left-hand side of this equation, $\rho + a + \lambda$ can be replaced by $\rho + a$, because $\rho + a \gg \lambda$, and then the diffusion flux can be expressed as

$$J = \frac{4\pi (\rho + a) D_\circ [c_\circ - c(\rho + 2a)]}{1 + [\lambda / (\rho + a)] \ln(\lambda / a)}. \tag{29}$$

In our context, as it has just been noticed, $\rho + a$ is appreciably larger than λ, and accordingly the logarithmic term in the denominator of this expression can be neglected, i.e.,

$$J \simeq 4\pi (\rho + a) D_\circ [c_\circ - c(\rho + 2a)]. \tag{30}$$

This expression indicates that the slowdown of diffusion near the NP surface is in fact negligible, because the main diffusion resistance takes place at $r \simeq 2\rho$, and in this region the diffusion coefficient is close to $D_\circ$.

In our analysis above, the protein diffusion coefficient has been described by employing expressions (20)–(22) corresponding to conventional hydrodynamics. *In vivo*, the diffusion can be slowed down due to the crowding effect [57,58]. At the simplest level, this effect can be taken into account by using expressions (20)–(22) in combination with the effective (reduced) friction coefficient. Following this line, we can employ Eq. (30) assuming $D_\circ$ to be the diffusion coefficient taking the crowding effect into account. In fact, Eq. (30) is the only one we need in the main text (Section 2).

Appendix B. Monte Carlo simulations

In principle, the kinetics of the protein-corona formation can be analyzed by using MC simulations. This technique allows one to scrutinize both spatial and temporal effects. Compared to the MF approximation, the corresponding results are, however, less transparent, and full-scale simulations of this category are beyond our present goals. Our attention is rather focused on illustration of the shortcomings of the MF approximation at high coverage. With this aim in mind, we performed temporal MC simulations of irreversible kinetically limited adsorption of spherically shaped proteins of one type (with radius of 1 nm) on a nanoparticle which was represented by a 20 × 20 nm^2 area with periodic boundary conditions. The corresponding kinetics [Fig. 7(a)] were simulated by using the standard Gillespie algorithm. In particular, the coordinates of the particle center for adsorption were chosen at random, an adsorption attempt was accepted if the distance between the

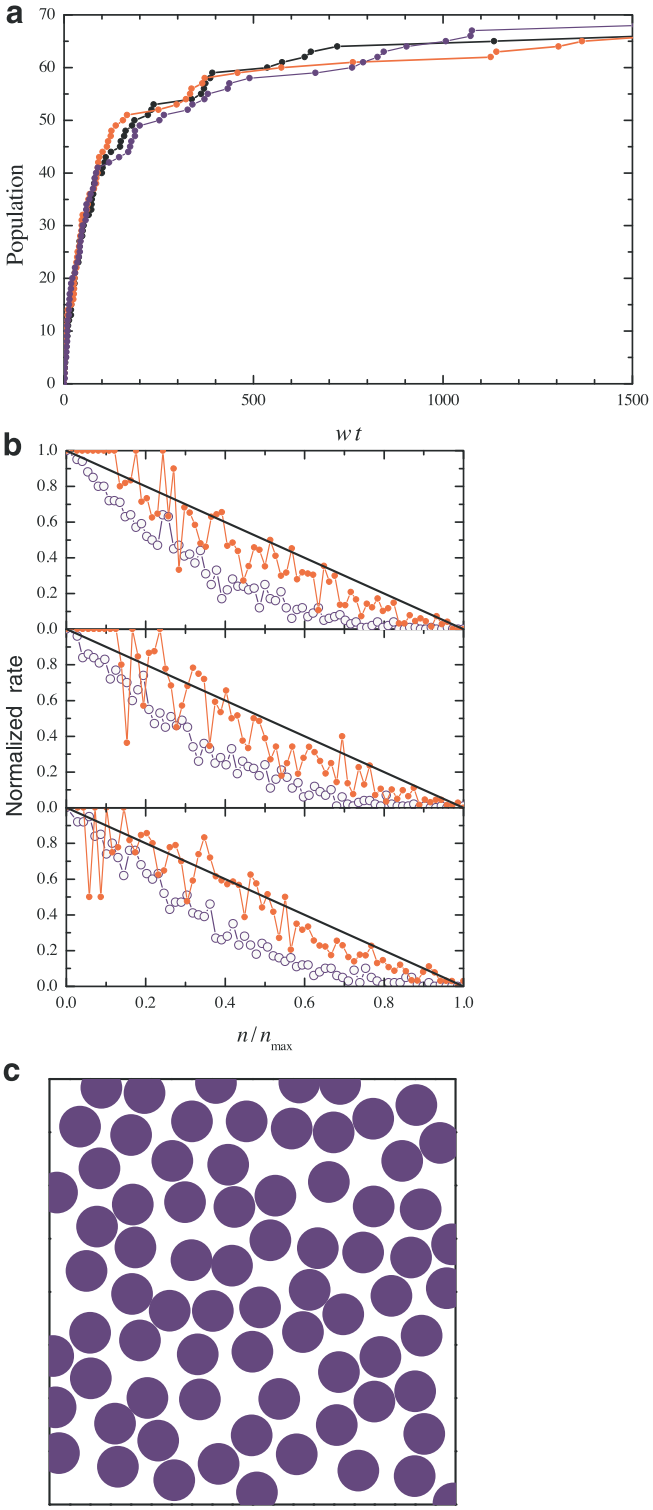

Fig. 7. Monte Carlo simulations of protein adsorption on a nanoparticle: (a) protein population as a function of time during three typical runs, (b) normalized average adsorption and denaturation rates (open and filled circles, respectively) as a function of n/n_{max} obtained for these runs (the solid line corresponds to the mean-field approximation), and (c) arrangement of proteins in the end of one of the runs.

chosen position for adsorption and the centers of already adsorbed proteins was larger than 2 nm, and after an attempt the time was incremented by $|\ln(\rho)|/w$, where w is the adsorption rate for the adsorbate-free surface [by analogy with Eq. (2), this rate can be represented as $w = Skc$, where S is the surface area, k is the adsorption rate constant (per unit area), and c is the protein concentration], and ρ ($0 < \rho \leq 1$) is a random number. To mimic rapid diffusion of adsorbed proteins, we performed 10^3 attempts of diffusion jumps after each adsorption attempt. For a jump, a protein was chosen at random, the likely coordinates of the protein center were selected at random locally at $x_i - \delta \leq x \leq x_i + \delta$ and $y_i - \delta \leq y \leq y_i + \delta$ (x_i and y_i are the initial coordinates, and $\delta = 0.5$ nm is the maximum jump length), and a jump attempt was accepted if the distance between the selected position and the centers of already adsorbed proteins was larger than 2 nm.

With the specification above, all the adsorbed proteins are in the same state, because the protein adsorption is considered to be not accompanied by denaturation. For any protein arrangement, we can, however, calculate the average adsorption rate as well as the average rate of denaturation which would take place if the latter process were allowed to occur [Fig. 7(b)]. The former rate was calculated by using 100 attempts of adsorption and defined as the fraction of the attempts which might be successful. The latter rate was calculated as the average rate of denaturation of adsorbed proteins. The denaturation was mimicked as an increase of the protein radius up to 2 nm (this process was assumed to be possible if there are no steric constraints for this increase), and the denaturation rate was identified with the fraction of the attempts which might be successful. All these attempts were tentative and were not accompanied by adsorption or denaturation. Physically, the average adsorption and denaturation rates calculated as defined above represent the rates normalized to the values corresponding to the protein-free nanoparticle. In the MF approximation, the average adsorption and denaturation rates calculated in a similar way can be identified with $1 - n/n_{\max}$, where n and $n_{\max}$ are the current and maximum protein population [cf. Eq. (2) and note that physically $n/n_{\max}$ represents Θ]. To illustrate the deviations from the MF approximation, the average MC adsorption and denaturation rates are shown as a function of $n/n_{\max}$, where $n_{\max}$ is the population in the end of the MC runs (a run was terminated after 10^3 sequential unsuccessful attempts of adsorption).

According to our simulations [Fig. 7(b)], the MF approximation overestimates the adsorption and denaturation rates at high coverage, and this effect is somewhat stronger in the case of adsorption. The overestimation is, however, not dramatic, and it is not expected to influence our qualitative conclusions.

References

[1] M. Malmsten, Biopolymers at Interfaces, Marcel Dekker, New York, 2003.
[2] J.J. Gray, The interaction of proteins with solid surfaces, Curr. Opin. Struct. Biol. 14 (2004) 110–115.
[3] T.S. Tsapikouni, Y.F. Missirlis, Protein-material interactions: from micro-to-nano scale, Mater. Sci. Eng. B 152 (2008) 2–7.
[4] M. Rabe, D. Verdes, S. Seeger, Understanding protein adsorption phenomena at solid surfaces, Adv. Colloid Interface Sci. 162 (2011) 87–106.
[5] A. Garland, L. Shen, X. Zhu, Mobile precursor mediated protein adsorption on solid surfaces, Prog. Surf. Sci. 87 (2012) 1–22.
[6] M. Kastantin, B.B. Langdon, D.K. Schwartz, A bottom-up approach to understanding protein layer formation at solid-liquid interfaces, Adv. Colloid Interface Sci. 207 (2014) 240–252.
[7] M. Ozboyaci, D.B. Kokh, S. Corni, R.C. Wade, Modeling and simulation of protein-surface interactions: achievements and challenges, Q. Rev. Biophys. 49 (2016) e4.
[8] V.P. Zhdanov, B. Kasemo, Monte Carlo simulations of the kinetics of protein adsorption, Surf. Rev. Lett. 5 (1998) 615–634.
[9] M. Rabe, D. Verdes, M. Rankl, G.R.J. Artus, S. Seeger, A comprehensive study of concepts and phenomena of the nonspecific adsorption of β-Lactoglobulin, ChemPhysChem 8 (2007) 862–872.
[10] I. Lundström, Models of protein adsorption on solid surfaces, Prog. Colloid Polym. Sci. 70 (1985) 76–82.
[11] R.D. Tilton, M. Malmsten, Mobility of Biomolecules at Interfaces, Biopolymers at Interfaces, Marcel Dekker, New York, 2003, pp. 221–258.
[12] L. Vroman, A.L. Adams, G.C. Fischer, P.C. Munoz, Interaction of high molecular weight kininogen, factor XII, and fibrinogen in plasma at interfaces, Blood 55 (1980) 156–159.
[13] C.F. Lu, A. Nadarajah, K.K. Chittur, A comprehensive model of multiprotein adsorption on surfaces, J. Colloid Interface Sci. 168 (1994) 152–161.
[14] M. Mahmoudi, I. Lynch, M.R. Ejtehadi, M.P. Monopoli, F.B. Bombelli, S. Laurent, Protein-nanoparticle interactions: opportunities and challenges, Chem. Rev. 111 (2011) 5610–5637.
[15] M.P. Monopoli, C. Åberg, A. Salvati, K.A. Dawson, Biomolecular coronas provide the biological identity of nanosized materials, Nat. Nanotechnol. 7 (2012) 779–786.
[16] C.D. Walkey, W.C.W. Chan, Understanding and controlling the interaction of nanomaterials with proteins in a physiological environment, Chem. Soc. Rev. 41 (2012) 2780–2799.
[17] S.R. Saptarshi, A. Duschl, A.L. Lopata, Interaction of nanoparticles with proteins: relation to bio-reactivity of the nanoparticle, J. Nanobiotechnol. 11 (2013) 26.
[18] C. Gunawan, M. Lim, C.P. Marquis, R. Amal, Nanoparticle-protein corona complexes govern the biological fates and functions of nanoparticles, J. Mater. Chem. B 2 (2014) 2060–2083.
[19] D. Docter, D. Westmeier, M. Markiewicz, S. Stolte, S.K. Knauer, R.H. Stauber, The nanoparticle biomolecule corona: lessons learned - challenge accepted? Chem. Soc. Rev. 44 (2015) 6094–6121.
[20] A.M. Dennis, J.B. Delehanty, I.L. Medintz, Emerging physicochemical phenomena along with new opportunities at the biomolecular-nanoparticle interface, J. Phys. Chem. Lett. 7 (2016) 2139–2150.
[21] S. Schöttler, K. Landfester, V. Mailänder, Controlling the stealth effect of nanocarriers through understanding the protein corona, Angew. Chem. Int. Ed. 55 (2016) 8806–8815.
[22] H.-W. Chen, C.-Y. Huang, S.-Y. Lin, Z.-S. Fang, C.-H. Hsu, J.-C. Lin, Y.-I. Chen, B.-Y. Yao, C.-M. J. Hu, Synthetic virus-like particles prepared via protein corona formation enable effective vaccination in an avian model of coronavirus infection, Biomaterials 106 (2016) 111–118.
[23] N.L. Anderson, N.G. Anderson, The human plasma proteome, Mol. Cell. Proteom. 1 (2002) 845–867.
[24] T. Cedervall, I. Lynch, S. Lindman, T. Berggård, E. Thulin, H. Nilsson, K.A. Dawson, S. Linse, Understanding the nanoparticle-protein corona using methods to quantify exchange rates and affinities of proteins for nanoparticles, Proc. NAS USA 104 (2007) 2050–2055.
[25] E. Casals, T. Pfaller, A. Duschl, G.J. Oostingh, V. Puntes, Time evolution of the nanoparticle protein corona, ACS Nano 4 (2010) 3623–3632.
[26] S. Khan, A. Gupta, C.K. Nandi, Controlling the fate of protein corona by tuning surface properties of nanoparticles, J. Phys. Chem. Lett. 4 (2013) 3747–3752.
[27] S. Tenzer, D. Docter, J. Kuharev, et al., Rapid formation of plasma protein corona critically affects nanoparticle pathophysiology, Nat. Nanotechnol. 7 (2013) 772–781.
[28] M. Wang, C. Fu, X. Liu, Z. Lin, N. Yang, S. Yu, Probing the mechanism of plasma protein adsorption on au and ag nanoparticles with FT-IR spectroscopy, Nanoscale 7 (2015) 15191–15196.
[29] J.E. Riviere, C. Scoglio, F.D. Sahneh, N.A. Monteiro-Riviere, Computational approaches and metrics required for formulating biologically realistic nanomaterial pharmacokinetic models, Comput. Sci. Discov. 6 (2013) 014005.
[30] D. Dell'Orco, M. Lundqvist, S. Linse, T. Cedervall, Mathematical modeling of the protein corona: implications for nanoparticulate delivery systems, Nanomedicine 9 (2014) 851–858.
[31] P. Vilaseca, K.A. Dawson, G. Franzese, Understanding and modulating the competitive surface-adsorption of proteins through coarse-grained molecular dynamics simulations, Soft Matter 9 (2013) 6978–6985.
[32] H. Lopez, V. Lobaskin, Coarse-grained model of adsorption of blood plasma proteins onto nanoparticles, J. Chem. Phys. 143 (2015) 243138.
[33] F. Tavanti, A. Pedone, M.C. Menziani, Competitive binding of proteins to gold nanoparticles disclosed by molecular dynamics simulations, J. Phys. Chem. C 119 (2015) 22172–22180.
[34] F. Tavanti, A. Pedone, M.C. Menziani, A closer look into the ubiquitin corona on gold nanoparticles by computational studies, New J. Chem. 39 (2015) 2474–2482.
[35] D. Dell'Orco, M. Lundqvist, C. Oslakovic, T. Cedervall, S. Linse, Modeling the time evolution of the nanoparticle-protein corona in a sody fluid, PLoS ONE 5 (2010) e10949.
[36] F.D. Sahneh, C. Scoglio, J. Riviere, Dynamics of nanoparticle-protein corona complex formation: analytical results from population balance equations, PLoS ONE 8 (2013) e64690.
[37] S. Angioletti-Uberti, M. Ballauff, J. Dzubiella, Dynamic density functional theory of protein adsorption on polymer-coated nanoparticles, Soft Matter 10 (2014) 7932–7945.
[38] J. Talbot, G. Tarjus, P.R.V. Tassel, P. Viot, From car parking to protein adsorption: an overview of sequential adsorption processes, Colloid Surf. A: Physicochem. Eng. Asp. 165 (2000) 287–324.
[39] J. Talbot, P. Schaaf, Random sequential adsorption of mixtures, Phys. Rev. A 40 (1989) 422–427.
[40] P. Meakin, R. Jullien, Random-sequential adsorption of disks of different sizes, Phys. Rev. A 46 (1992) 2029–2038.
[41] P. Meakin, R. Jullien, Random sequential adsorption of spheres of different sizes, Physica A 187 (1992) 475–488.

[42] C.M. Roth, A.M. Lenhoff, Electrostatic and van der Waals contributions to protein adsorption: computation of equilibrium consthnts, Langmuir 9 (1993) 962–972.
[43] C.M. Roth, A.M. Lenhoff, Electrostatic and van der Waals contributions to protein adsorption: comparison of theory and experiment, Langmuir 11 (1996) 3500–3509.
[44] Z. Adamczyk, Particle adsorption and deposition: role of electrostatic interactions, Adv. Colloid Interface Sci. 100–102 (2003) 267–347.
[45] Z. Adamczyk, M. Nattich-Rak, M. Sadowska, A. Michna, K. Szczepaniak, Mechanisms of nanoparticle and bioparticle deposition - kinetic aspects, Colloid Surf. A: Physicochem. Eng. Asp. 439 (2013) 3–22.
[46] J.P.K. Doye, W.C.K. Poon, Protein crystallization in vivo, Curr. Opin. Colloid Interface Sci. 11 (2006) 40–46.
[47] A.C. Dumetz, A.M. Chockla, E.W. Kaler, A.M. Lenhoff, Effects of pH on protein-protein interactions and implications for protein phase behavior, Biochim. Biophys. Acta 1784 (2008) 600–610.
[48] J.-H. Choi, S.-O. Kim, E. Linardy, E.C. Dreaden, V.P. Zhdanov, P.T. Hammond, N.-J. Cho, Adsorption of hyaluronic acid on solid supports: role of pH and surface chemistry in thin film self-assembly, J. Colloid Interface Sci. 448 (2015) 197–207.
[49] M. von Smoluchowski, Versuch einer mathematischen theorie der koagulationskinetik kolloider lösnngen, Z. Phys. Chem. 92 (1917) 129–168.
[50] F.C. Collins, G.E. Kimball, Diffusion-controlled reaction rates, J. Colloid Sci. 4 (1949) 425–437.
[51] O.G. Berg, On diffusion controlled dissociation, Chem. Phys. 31 (1978) 47–57.
[52] D.T. Gillespie, A. Hellander, L.R. Petzold, Perspective: stochastic algorithms for chemical kinetics, J. Chem. Phys. 138 (2013) 170901.
[53] P. Mereghetti, D. Kokh, J.A. McCammon, R.C. Wade, Diffusion and association processes in biological systems: theory, computation and experiment, BMC Biophys. 4 (2011) 2.
[54] M.A. Bevan, D.C. Prieve, Hindered diffusion of colloidal particles very near to a wall: revisited, J. Chem. Phys. 113 (2000) 1228.
[55] Y. Kazoe, M. Yoda, Measurements of the near-wall hindered diffusion of colloidal particles in the presence of an electric field, Appl. Phys. Lett. 99 (2011) 124104.
[56] V.P. Zhdanov, The effect of viscosity on the rate of diffusion-limited association of nanoparticles, J. Chem. Phys. 143 (2015) 166102.
[57] T. Misteli, Physiological importance of RNA and protein mobility in the cell nucleus, Histochem. Cell Biol. 129 (2008) 5–11.
[58] J.T. Mika, B. Poolman, Macromolecule diffusion and confinement in prokaryotic cells, Curr. Opin. Biotechnol. 22 (2011) 117–126.